



Mass-independent isotopic signatures of volcanic sulfate from three supereruption ash deposits in Lake Tecopa, California

Erwan Martin*, Ilya Bindeman

Department of Geological Sciences, 1272 University of Oregon, Eugene OR 97403, USA

ARTICLE INFO

Article history:

Received 10 October 2008

Received in revised form 24 February 2009

Accepted 2 March 2009

Available online 10 April 2009

Editor: R.W. Carlson

Keywords:

oxygen and sulfur isotopes
isotopic mass-independence
sulfate
aerosols
supereruption
ozone depletion

ABSTRACT

Hundreds to thousands of megatons of sulfur dioxide released by supereruptions can change chemical and physical properties of the atmosphere and thus induce climate perturbations. We present oxygen and sulfur isotope analyses of sulfate in 48 volcanic ash samples, and 26 sediment samples from dry lake beds in the Tecopa basin, California, USA. These ash layers represent three supereruptions, including the 0.64 Ma Lava Creek Tuff, 2.04 Ma Huckleberry Ridge Tuff and 0.76 Ma Bishop Tuff.

Mass-independent oxygen signatures ($\Delta^{17}\text{O}$ up to 2.26‰) that are present in these ash units, and not in associated sediments, indicate oxidation of volcanic SO_2 by mass-independent ozone and its products. In this study, we consider the formation, deposition, preservation and dilution of mass-independent volcanic sulfate (MIVS). Using the isotopic compositions of the sulfates, we construct a mixing model that demonstrates that the main source of sulfate in Lake Tecopa is mass-dependent sediment-derived sulfate (MDSDS, >77%). However, ash beds still preserve up to 23% of MIVS that initially had undiluted $\Delta^{17}\text{O}$ value around 8‰, and $\Delta^{33}\text{S}$ as low as -0.35% , and $\Delta^{36}\text{S}$ up to 1.08‰. Therefore, despite potential dilution by MDSDS, the MIVS signatures can be preserved in the geologic record for few million years, if deposited as gypsum in arid environments, alkaline or saline lake.

The oxygen and sulfur mass-independent signatures of the volcanic sulfates indicate that photolysis and oxidation of volcanic SO_2 has been achieved in the upper atmosphere. Since only supervolcanic eruptions were shown to generate massive amount of mass-independent sulfate, it requires that up to 20–60% of the global ozone layer is consumed as a result of supervolcanic SO_2 released. This may occur as a result of a strong physical and chemical degradation of the tropopause; we speculate that the distinction between the high-troposphere and the low-stratosphere, at least locally, could be erased by supereruptions, and recorded by MIVS.

© 2009 Elsevier B.V. All rights reserved.

1. Introduction

Volcanic eruptions of large magnitudes (called supereruptions) release many megatons of volcanic ash and SO_2 gas, which upon turning into H_2SO_4 aerosols, reflect solar radiation and cause Earth's surface cooling and stratosphere heating (e.g. Robock, 2000 and references therein). Slow oxidation of SO_2 in the stratosphere leads to a global climate cool that lasts years to decades (e.g. Blong, 1984; Zielinski et al., 1996; Robock and Oppenheimer, 2003). Both oxygen and sulfur isotopic compositions of volcanic sulfates provide insight into the pathways of SO_2 oxidation and residence time in the atmosphere.

Volcanic plumes from large eruptions can reach high altitudes (20–40 km). At such altitude, most oxygen-bearing molecular species (oxyanions) in the Earth's atmosphere exhibit mass-independent isotope behavior (e.g. Thiemens, 2006 and references therein), with ozone $\Delta^{17}\text{O}$ values of up to +10 to +80‰ (+32‰ on average, e.g. Krankowsky et al.,

2000). The ^{17}O -excess¹ measured in volcanic sulfate from large eruptions (Bao et al., 2003; Bindeman et al., 2007) could ultimately be inherited from the ozone.

The volcanic sulfate has been isotopically studied after leaching of volcanic ash samples (e.g. Bao et al., 2003; Bindeman et al., 2007), and by extracting volcanic ash from ice cores from Antarctica (e.g. Savarino et al., 2003a,b; Baroni et al., 2007). The ice core sulfates show mass-independent behavior not only of oxygen, but also sulfur isotopes. The sulfur mass-independence require photodissociation of SO_2 or SO_3 by <310 nm short wave UV radiation (Farquhar et al., 2000; Farquhar et al., 2001) in the upper stratosphere, where the O_3 shield is not thick enough to prevent it (e.g. Farquhar and Wing, 2003).

Bindeman et al. (2007) showed that sulfates from distal ash deposits of the largest caldera-forming eruptions ($\geq 600 \text{ km}^3$) for the past 2 Ma possess positive and high $\Delta^{17}\text{O}$ of 0.7 to 3.5‰, while sulfate from smaller eruptions ($\leq 10 \text{ km}^3$) show $\Delta^{17}\text{O} < 0.3\%$. Bao et al. (2003) measured

¹ The ^{17}O -excess, or deviation from the terrestrial mass fractionation line ($\delta^{17}\text{O} \approx 0.52 \times \delta^{18}\text{O}$) is expressed as $\Delta^{17}\text{O} = \delta^{17}\text{O} - 0.52 \times \delta^{18}\text{O}$; see Miller (2002) for different formulations.

* Corresponding author.

E-mail address: ermartin@uoregon.edu (E. Martin).

$\Delta^{17}\text{O} < 0.2\%$ in sulfate leached from products of modern small eruptions, but reported the record high $\Delta^{17}\text{O}$ value of $+5.84\%$ in sulfate from 28 Ma ash layers in western Nebraska from an unidentified, sulfur-rich and large-volume eruption. The high- $\Delta^{17}\text{O}$ in sulfates from large eruptions have been interpreted as reflecting the volcanic SO_2 oxidation by ozone-derived radicals in the troposphere (e.g. “dry fog”, Bao et al., 2003) or stratosphere (e.g. Bindeman et al., 2007). Savarino et al. (2003a) additionally reported $\Delta^{17}\text{O} = 4.7\%$ in stratospherically-processed sulfate collected in ash deposits from the medium-scale (10 km^3) 1991 Mt Pinatubo eruption in the Antarctica ice.

While previous studies created an important framework, they provided insufficient details on the formation, deposition and preservation of mass-independent volcanic sulfates (MIVS). In this paper, we present a detailed study of sulfate extracted from volcanic ash and enclosing sediments in the presently dry Lake Tecopa, near Death Valley in California, USA. This sedimentary basin deposit contains ash layers from the three largest eruptions that occurred in the western USA during the past 2 Ma: two eruptions from Yellowstone: the 0.64 Ma, 1000 km^3 Lava Creek Tuff (LCT) and the 2.04 Ma, 2500 km^3 , Huckleberry Ridge Tuff (HRT), and one eruption from the Long Valley caldera: the 0.76 Ma, 750 km^3 Bishop tuff (BT). We performed analyses of $\delta^{18}\text{O}$, $\Delta^{17}\text{O}$, and $\delta^{34}\text{S}$ in extracted sulfates and measurement of ash, sulfate and CaCO_3 concentrations. We additionally employ and reinterpret $\Delta^{33}\text{S}$ and $\Delta^{36}\text{S}$ data from Bindeman et al. (2007) as being mass-independent. Based on petrographic observations and measured isotopic values, we estimate the proportion of sedimentary and volcanic sulfate sources in Lake Tecopa and discuss the preservation of oxygen mass-independent volcanic sulfates (MIVS) in sedimentary records of intermountain basins. By linear algebra and mass-balance, we estimate the primary volcanic sulfate $\Delta^{17}\text{O}$, $\Delta^{33}\text{S}$ and $\Delta^{36}\text{S}$ values, and speculate on the quantity of atmospheric ozone consumed in the process of volcanic sulfate formation during these three supereruptions.

2. Geological setting and sampling

The presently dry Lake Tecopa is located in the major intermountain basin to the southeast of Death Valley (Fig. 1). From the

Pliocene to middle Pleistocene, Lake Tecopa oscillated between playa to shallow-lake conditions and even during its deepest stages (5–10 m) it remained both saline and alkaline (e.g. Morrison, 1999 and references therein). In this lake, the sedimentary deposits are 100 meters thick and contain at least 15 ash layers (Sheppard and Gude, 1968; Strakey and Blackmon, 1979; Hillhouse, 1987) that were deposited by airfall and redeposited into the lake by fluvial processes. Among these volcanic deposits three are meters-thick and are continuously present across the lake: the 0.64 Ma LCT, 0.76 Ma BT, and 2.04 Ma HRT (Figs. 1 and 2). The LCT ash bed is usually 2–2.5 m thick, reaching up to 3–4 m close to the town of Shoshone; (Fig. 2), the BT ash layer is commonly 1–1.5 m thick, and the affected by K-feldspar diagenesis HRT ash bed is the thinnest (0.5–0.7 m; Fig. 2 and 3). We estimate that these ash layers represent 15–20 vol.% of the Lake Tecopa sedimentary volume studied here (Fig. 3).

We collected 48 samples from LCT, BT and HRT ash beds and 26 samples from enclosing sediments along 18 different profiles. In each sampling location we collected ash every 10–30 cm from the bottom to the top of each layer, and extending into the sediments from 0.5–2 m below and above each ash beds (Table 1 and Fig. 3). The majority of samples were collected in the northern part of the Tecopa basin, where the ash layers are best exposed and not affected by diagenetic processes (e.g. Sheppard and Gude, 1968), as verified by fresh ash shards that are optically isotropic. A few samples were collected in the zeolite and K-feldspar diagenetic facies for comparison (Fig. 2).

3. Methods

Sulfate was leached from 40–80 g of samples with HCl-acidified solution ($\text{pH} = 1\text{--}2$) and precipitated as barite (BaSO_4) by adding barium chloride (BaCl_2) to the solution while evaporating at $T < 80^\circ\text{C}$. Barite was purified from potential nitrate contamination by repeated dissolution–reprecipitation with chelating DTPA agent, because adsorbed nitrate contamination was suggested to influence the barite $\Delta^{17}\text{O}$ values (e.g. Bao, 2006). In this study, like an earlier study by Bindeman et al. (2007), nitrate contamination was found to be minor

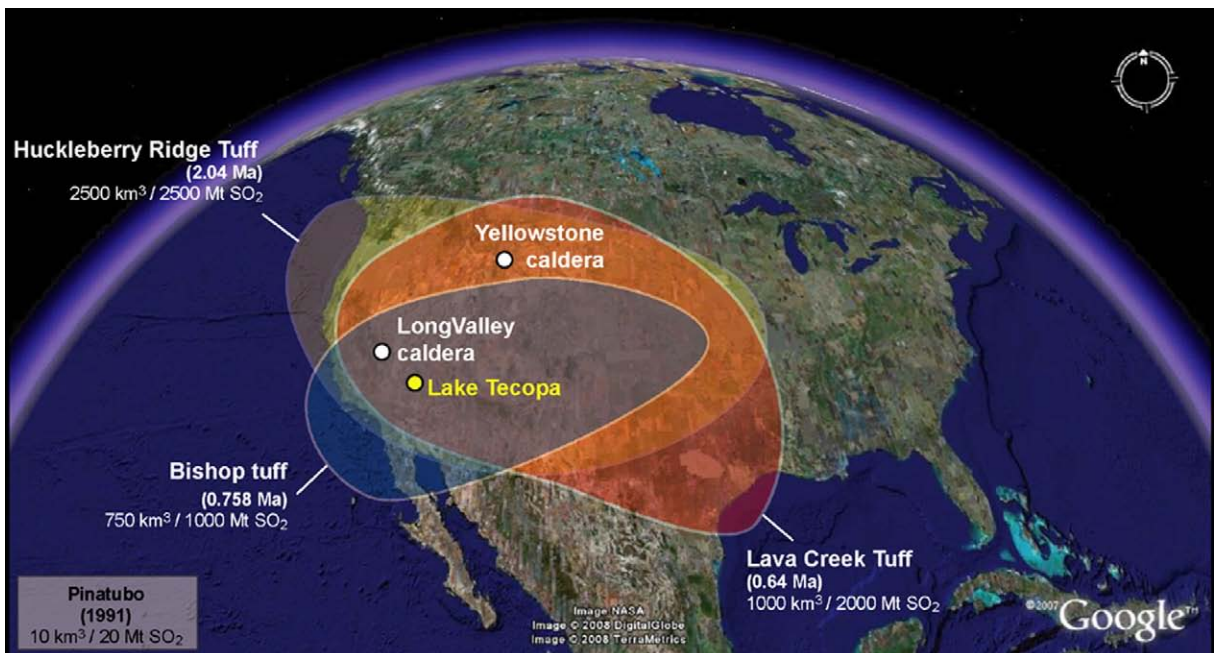


Fig. 1. Map of North America showing the distribution of air-fall deposit from supervolcanic eruptions of Yellowstone: Huckleberry Ridge Tuff (2.04 Ma) and Lava Creek Tuff (0.64 Ma) and Long Valley: Bishop Tuff (0.76 Ma). The location of the dry lake Tecopa is indicated by a white labeled circle.

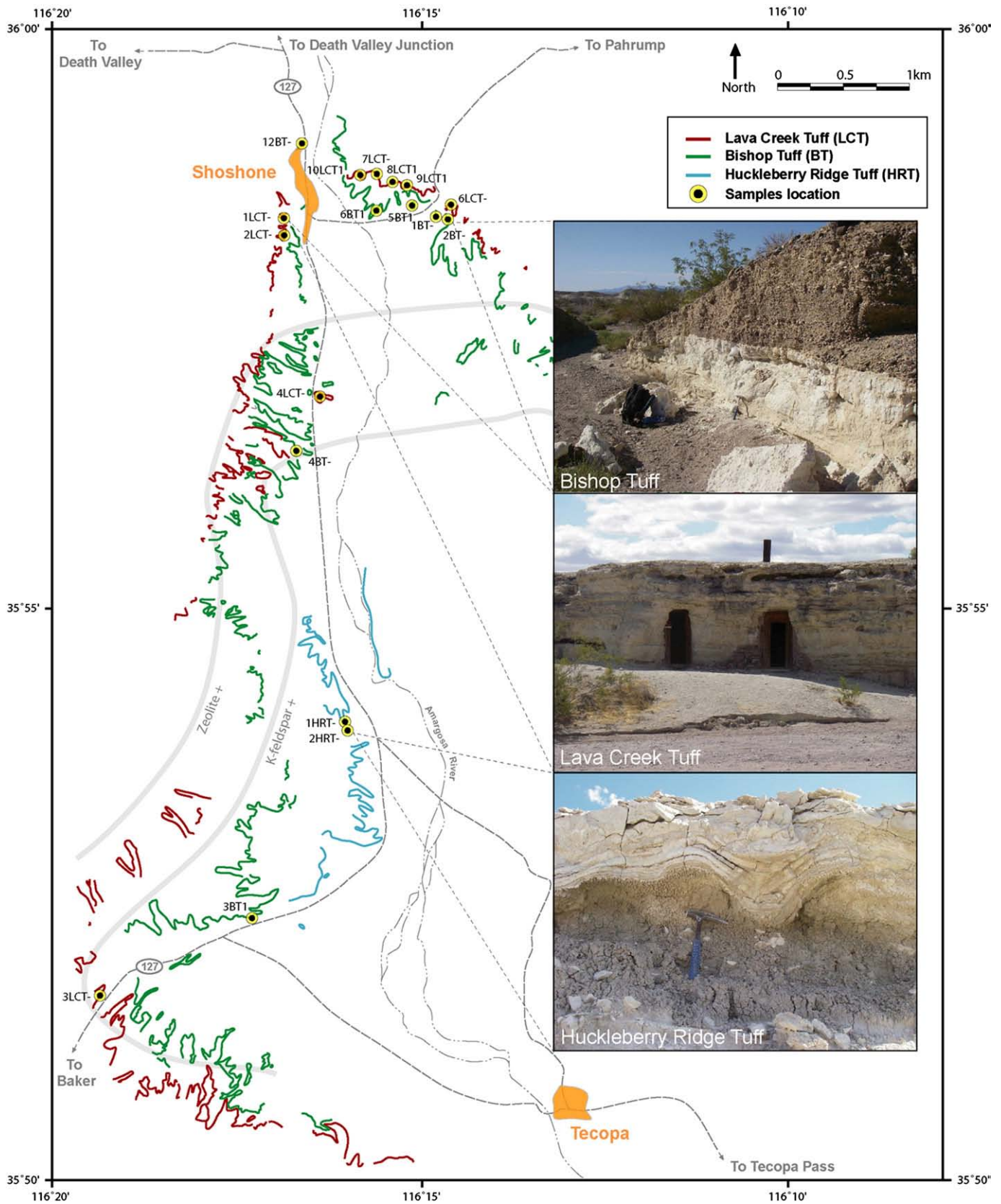


Fig. 2. Map of the dry Lake Tecopa showing outcrops of the Huckleberry Ridge Tuff, Lava Creek Tuff and Bishop Tuff ash layers (Hillhouse, 1987) and our sampling localities. The diagenetic facies (zeolite and K-feldspar) are from Sheppard and Gude (1968). Insets show field photographs of the studied ash layers.

(<2–3 wt.%) and does not affect $\Delta^{17}\text{O}$ significantly. Indeed, measured $\Delta^{17}\text{O}$ values from 16 untreated and treated barite plot less than 0.1‰ from the 1:1 line (Supplementary material).

Oxygen isotopes from 4–7 mg of extracted barite powder were analyzed at the Stable Isotope Laboratory at the University of Oregon by laser fluorination, using methods similar to Bao and Thiemens

(2000). Extracted O₂ gas was then frozen in a molecular sieve (zeolite 13 Å) and run in a dual inlet mode in a Finnigan MAT253 mass spectrometer. Some samples were frozen in both a single and double molecular sieve (zeolite 13 Å) trap system to check for potential NF⁺ contamination that can affect mass 33 (e.g. Rumble et al., 1997; Pack et al., 2007; Supplementary material). We found such contamination to be negligible.

Sample duplicates, and replicates of barite international standard NBS127 ($n=7$) and an in-house standard (IBO4-13; $n=12$) give a reproducibility (in 2σ) of $\delta^{18}\text{O} \pm 0.6\%$, $\delta^{17}\text{O} \pm 0.3\%$ and $\Delta^{17}\text{O} \pm 0.05\%$. The 35–45% O₂ yield during barite laser fluorination leads to low- $\delta^{18}\text{O}$ values, therefore based on the certified $\delta^{18}\text{O}$ value of NBS127 ($\delta^{18}\text{O} = 8.6\%$), we applied a correction factor of +0.81% for all analyzed samples. Notice that this correction, which is a mass-independent parameter, does not affect $\Delta^{17}\text{O}$ values. Day-to-day variations were also monitored by the GMG garnet standard ($\delta^{18}\text{O} = 5.75\%$). Repeated leaching and analysis from the same samples yielded external errors (in 2σ) of the whole method better than $\delta^{18}\text{O} \pm 1.2\%$ and $\Delta^{17}\text{O} \pm 0.1\%$ (Supplementary material).

Sulfur isotopes were analyzed via an elemental analyzer in the stable isotope laboratory at the University of Maryland. Multiple analyses of NBS127 give $\delta^{34}\text{S} = -8.37\% \pm 0.05$ (in 2σ) and based on the certified value (21.1%) a correction factor of +29.47% was applied for all samples.

In addition to microscopic examination, we investigated sulfate size, position, and morphology at the Smithsonian Institution of Washington DC. SEM imaging and X-ray mapping of one ash (LCT8) and one sediment (2BT + 1) sample used the FEI Nova NanoSEM 600 variable pressure ultra high resolution SEM fitted with ThermoNoran energy dispersive X-ray detector (EDS), and we additionally characterized these samples by X-ray diffraction using a Rigaku D/MAX Rapid microdiffractometer.

4. Results

4.1. Petrography of sediment and ash layers

Lake Tecopa sediments mainly consist of lacustrine mudstone including clay, silt and sand (Sheppard and Gude, 1968; Hillhouse, 1987; Fig. 3). Some claystones are interbedded whereas sandstones appear as lenses in the mudstone. X-ray diffraction analyses performed on sediment (sample 2BT + 1) led to the identification of calcite, clay minerals (montmorillonite and sepiolite), quartz, albite and micas. Authigenic zeolite and K-feldspar are also present in sediments as well as in ash located close to the center of the Tecopa basin, but absent in the northern and shallowest part of the basin (Fig. 2).

A macroscopic and microscopic petrographic investigation of each ash layer showed that the lower contact of the volcanic deposit is sharp, created by a massive and rapid air fall into the Tecopa basin. By contrast, the upper contact is gradual, showing progressive mixing of ash with the overlying sediments (Fig. 3). Locally, the upper part of the ash layers is seen as being fluvially reworked, and in other places, the volcanic deposit is cemented by carbonates that result in hard beds. The proportion of birefringent lithics across the optically isotropic ash bed was estimated with a petrographic microscope for most samples (Fig. 3), and changes gradually from the bottom to the top of each ash layer. We identified some of these lithics, via X-ray diffraction analyses, as halite and montmorillonite (sample LCT8). The sediment below the ash layers is always ash-poor (<5%). The bottom of each ash layer consists of almost pure glass (>95% of 100–200 μm glass shards) and a very high ash proportion (>90%) remains across most of the ash layer (Fig. 3). At the top, where there is some cross-bedding and evidence of fluvial reworking of the volcanic deposit, the proportion of ash decreases progressively from 70 to 30%. The overlying sediment is heavily contaminated with ash (10–30%).

In some places, the overlying sediment also contains ash-rich lenses (>50%; Fig. 3).

4.2. Sulfate appearance and concentrations

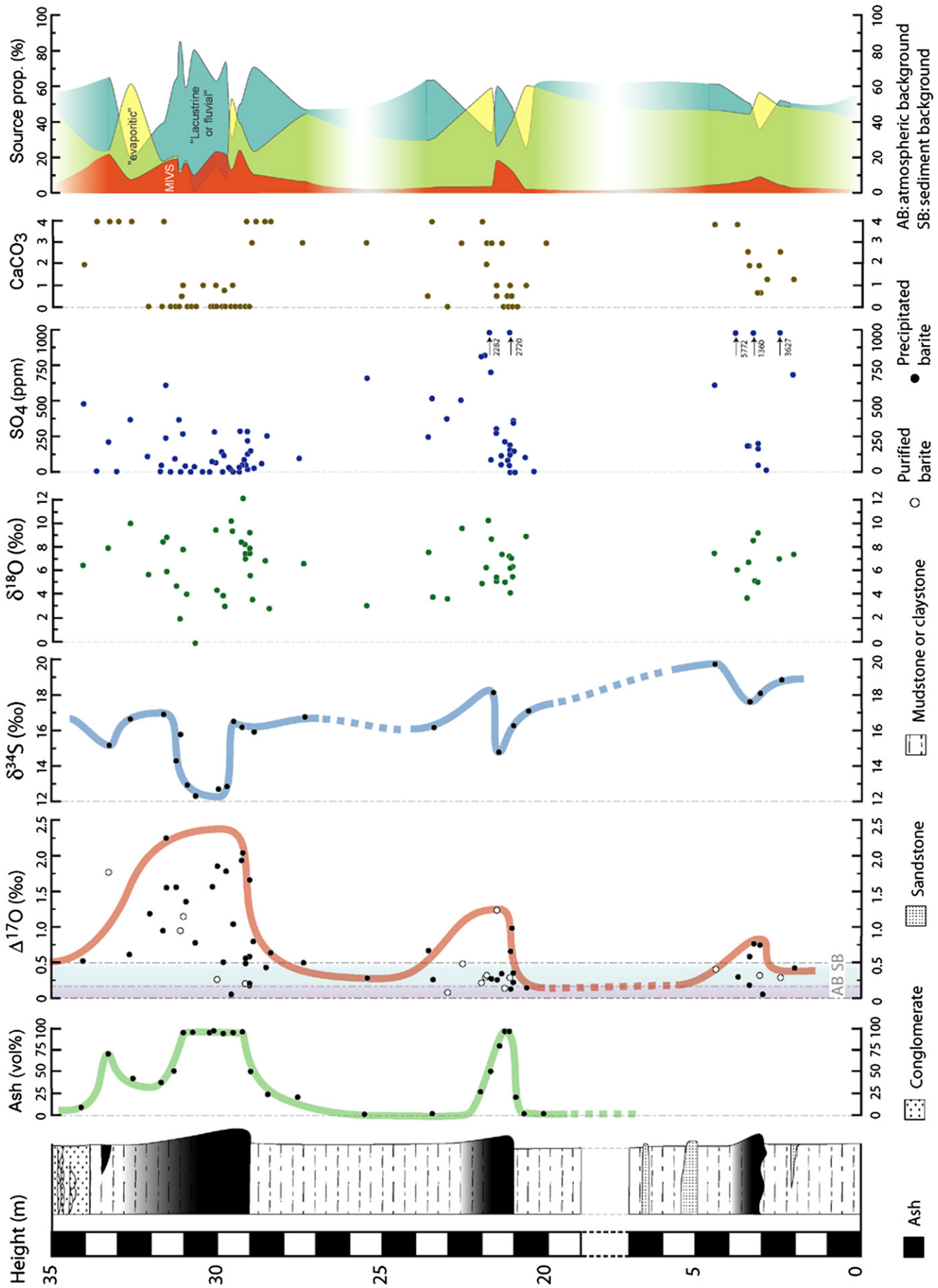
SEM imaging and X-ray mapping (100 $\mu\text{m} \times 100 \mu\text{m}$) of one ash (LCT8) and one sediment (2BT + 1) samples succeeded in identifying gypsum (or anhydrite) particles between 1 and 10 μm , but generally 3–5 μm in size (Fig. 4). Likewise, Bindeman et al. (2007) reported CaSO₄ particles in their samples. High magnification scanning of individual gypsum particles in ash samples, demonstrate that the sulfates occur as reprecipitated clumps (Fig. 4).

In 85% of the samples, sulfate concentration was high and variable: ash layers contained 304 ± 151 (2σ) ppm SO₄, and sediments contained 653 ± 482 (2σ) ppm SO₄ (Table 1 and Fig. 3). It is noteworthy that in a single ash layer, the sulfate content varies irregularly, both vertically and laterally. For instance in the LCT profile 1 (Fig. 2; Table 1), SO₄ concentration ranges between 30 ppm and 365 ppm, and only in two samples (1LCT2 and 1LCT5), sulfate concentration was too low for extraction (<7 ppm; Table 1). Similarly, when comparing LCT profile 1 and profile 2 (Fig. 2 and Table 1), which are a few hundred meters apart, 75% of the samples from profile 1 have significant amount (>7 ppm) of sulfate while this is the case for only 10–15% in the profile 2. Overall, in only 15% of the samples, the sulfate (SO₄) concentration was too low for extraction. However, since the neighboring samples have plentiful sulfate it appears that highly variable sulfate concentration is due to very recent secondary leaching and loss. As an example, we did not find any sulfate in samples from 1 m thick ash layer from the Toba supereruption (74 ka) in Malaysia. It is likely that the wet climate in this region had naturally leached sulfate from ash. Likewise, recent erosion and leaching probably affected the Lake Tecopa sulfate distribution. However, secondary leaching is a mass-dependent process, unable to change the sulfate mass-independent $\Delta^{17}\text{O}$ signature. Moreover, it has been demonstrated that leaching and sulfate loss does not significantly change the sulfate $\delta^{18}\text{O}$ and $\delta^{34}\text{S}$ (e.g. Van Stempvoort and Krouse, 1994; Khademi et al., 1997).

4.3. $\Delta^{17}\text{O}$, $\delta^{18}\text{O}$ and $\delta^{34}\text{S}$ values of sulfate

Overall, the sulfates extracted from the ash layers exhibit large ranges in oxygen and sulfur isotopic compositions: the $\delta^{18}\text{O}$ ranges from 0.0 to 12.1‰ while the $\delta^{34}\text{S}$ ranges from 6.1 to 19.8‰. The sediment-extracted sulfates show a similarly large diversity: $\delta^{18}\text{O}$ ranges from 2.8 to 10.0‰ and $\delta^{34}\text{S}$ from 14.3 to 19.7‰ (Table 1 and Fig. 3). The highest $\Delta^{17}\text{O}$ values, up to 2.26‰ (Fig. 3 and 5), were measured in sulfates from ash whereas sulfate from the sediments has usually $\Delta^{17}\text{O} < 0.5\%$. The lower contact between ash layers and underlying sediment is characterized by a sharp increase of the $\Delta^{17}\text{O}$ values, in agreement with the ash proportion (Fig. 3). The maximum $\Delta^{17}\text{O}$ were usually measured in the lower part of ash layers, where ash concentration exceeds 95% of the sample (Fig. 3). The maximum $\Delta^{17}\text{O}$ value gradually decreases to the top of ash beds and is roughly correlated with the proportion of ash in samples (Fig. 3). Additionally, high $\Delta^{17}\text{O}$ values, up to 1.78‰, were measured in fluvially-redeposited ash-rich sediment lenses as observed on top of the LCT ash layers (Fig. 3). The sediment background $\Delta^{17}\text{O}$ values are in the 0.15 to 0.5‰ range, and remain approximately constant for 2 Ma in the studied sections. Progressively older and less thick ash layers exhibit a decrease in the maximum measured $\Delta^{17}\text{O}$ values: $\Delta^{17}\text{O} = 2.26\%$ in the 0.64 Ma LCT, $\Delta^{17}\text{O} = 1.25\%$ in the 0.76 Ma BT, and $\Delta^{17}\text{O} = 0.76\%$ in the 2.04 Ma HRT (Fig. 3).

It appears in these studied profiles that the main process that affects sulfate isotopic values, and $\Delta^{17}\text{O}$ in particular, is sediment-ash sulfate mixing. The pattern of the inferred mutual cross-contamination is not simple since sediments contain on average twice the amount of



sulfate as ash. The fresh ash samples generally have sulfate concentration lower than 400 ppm and high $\Delta^{17}\text{O}$ ($>0.5\%$), while sediments are usually sulfate-richer (>400 ppm) and have lower $\Delta^{17}\text{O}$ values ($<0.5\%$; Fig. 6). This pattern alone suggests volcanic origin of high $\Delta^{17}\text{O}$ in ash. Sulfate from ash, when mixed with sediments yields lower $\Delta^{17}\text{O}$ ($<0.6\%$) than in fresh ash, while the sediments contaminated by ash have higher $\Delta^{17}\text{O}$ than the sediment background (0.5%). While $\Delta^{17}\text{O}$ in ash-uncontaminated sediments is systematically lower than 0.5% , the ^{17}O -excesses are still significantly higher than $0.0 \pm 0.1\%$ as would be expected for sediments derived from mass-dependent sources. There is a possibility that mass-independent signatures are coming from long-term atmospheric aerosol deposition (e.g. Bao et al., 2001), however the time-averaged amount of such precipitation in the Tecopa basin would not generate $\Delta^{17}\text{O}$ higher than 0.2% (see below).

Other stable isotope parameters and concentrations exhibit variable levels of correlation with lithology: the $\delta^{34}\text{S}$ decreases in ash layers (Fig. 3), and anticorrelates with $\Delta^{17}\text{O}$ (Fig. 5); less clear correlation is observed with sulfate concentrations and $\delta^{18}\text{O}$ (Fig. 3). Carbonate concentration is lower in ash beds than in sediment (Fig. 3), and this is most likely due to the fact that we sampled the freshest ash.

Finally, no systematic correlation between $\Delta^{17}\text{O}$ and the degree of diagenesis has been observed (Table 1 and Fig. 2): a negative correlation for LCT samples and slightly positive for BT samples. Diagenesis is a mass-dependent process incapable of changing the $\Delta^{17}\text{O}$ values of sulfates.

5. Discussion

The following discussion addresses 1) the sources of sulfate present in the studied sedimentary sections, 2) the mechanisms of incorporation of volcanic sulfate into ash beds, 3) the preservation of oxygen mass-independent volcanic sulfate in a sedimentary basin under arid environment conditions, 4) the sulfur mass-independent signature and 5) atmospheric perturbations due to the release of large amounts of volcanic SO_2 , as revealed by its $\Delta^{17}\text{O}$ signature.

5.1. Sulfate sources

5.1.1. Mass-independent sulfate

In the arid environment of Lake Tecopa, the main source of initial ^{17}O -excess in sediment is from atmospheric sulfate aerosols. Bao and Reheis (2003) measured maximum $\Delta^{17}\text{O}$ values of 0.85 – 0.44% in sulfate collected in dust traps. Long-term accumulation of sulfate is exemplified by desert varnishes, which have $\Delta^{17}\text{O}$ values of up to 0.6 – 0.8% (Bao et al., 2001). Sulfate in desert varnishes allow assessment of atmospheric accumulation rates and $\Delta^{17}\text{O}$ values during a few hundred thousand years. Using the maximum accumulation rate of $5 \mu\text{m}/1000$ years for a desert varnish (Dorn, 1998) that contains 0.6 wt.% of mass-independent SO_4 (Bao et al., 2001), the deposition rate of mass-independent atmospheric sulfates is $30 \mu\text{m}/\text{Ma}$. By contrast, in Lake Tecopa, playa or alluvial sediments had an average accumulation rate of ~ 40 m/Ma (Morrison, 1999), or ~ 24 mm/Ma of the equivalent sulfate (considering ~ 600 ppm in average in sediment). If we assume that atmospheric sulfate precipitation is 100 times greater than that recorded in varnishes, then the atmospheric mass-independent sulfate represents 12.5% (75 ppm) of the sediment sulfate. Therefore, considering the maximum $\Delta^{17}\text{O}$ value of 1.2% (most likely $\sim 0.5\%$ on average) for atmospheric aerosols at Death Valley (Bao et al., 2001), the resulting $\Delta^{17}\text{O}$ of sediment sulfate is $<0.2\%$. Thus, the atmospheric

mass-independent signature is extensively diluted by non-atmospheric mass-dependent sulfate leading to negligible ^{17}O -excess in sediments. This is supported by $\Delta^{17}\text{O}$ as low as 0.2% in modern day evaporitic sulfate at the surface of Lake Tecopa (Bindeman et al., 2007).

We conclude that long term atmospheric deposition is incapable of explaining the large concentration of high $\Delta^{17}\text{O}$ sulfate in ash layers, which must be volcanic in origin. A few hundreds ppm SO_4 deposited in a few years into a meter-thick ash layers requires a sulfate accumulation rate $\sim 10^4$ times greater than the average atmospheric sulfate aerosol accumulation rate estimated above. Indeed, this can be achieved by large scale volcanic eruptions.

In Lake Tecopa, the highest $\Delta^{17}\text{O}$ measured in ash sulfates is 2.26% , but this $\Delta^{17}\text{O}$ value was diluted by mass-dependent sedimentary sulfate ($\Delta^{17}\text{O} \sim 0\%$). How high was the initial undiluted $\Delta^{17}\text{O}$ signature of those ash layers? If we assume that the overall amount of sulfate in the lake remained approximately constant through time, and use the estimate that ash represents 15 – 20 vol.% of sediments in the Lake Tecopa basin, and assume that the mass-independent signature of sulfate in sediments was derived from the ash, we can estimate the following initial range of $\Delta^{17}\text{O}$ in the freshly deposited layers of volcanic ash:

$$X_{(\text{ash})I} \times \Delta^{17}\text{O}_{(\text{ash})I} + X_{(\text{sed})I} \times \Delta^{17}\text{O}_{(\text{sed})I} = X_{(\text{ash})F} \times \Delta^{17}\text{O}_{(\text{ash})F} + X_{(\text{sed})F} \times \Delta^{17}\text{O}_{(\text{sed})F}$$

I: initial and *F*: final

X: sulfate proportion derived from sulfate concentration ($X_{(\text{ash})F} = 7.6\%$ and $X_{(\text{sed})F} = 92.4\%$)

$$X_{(\text{ash})F} = X_{(\text{ash})I} \text{ and } X_{(\text{sed})F} = X_{(\text{sed})I}$$

The application of this simple mass-balance gives an initial $\Delta^{17}\text{O}$ for the MIVS between 6.5% and 8.5% . This estimate approaches the theoretical maximum $\Delta^{17}\text{O}$ value of 8.0% that we discuss below. It is thus apparent that the initially large $\Delta^{17}\text{O}$ signal was diluted in ash layers while increasing $\Delta^{17}\text{O}$ up to 0.5% in sediments.

5.1.2. Mass-dependent sulfates

Sedimentary sulfate derived from weathering and oxidation of igneous sulfides during a few Ma should have $\Delta^{17}\text{O}$ value close to 0% and variable $\delta^{34}\text{S}$ and $\delta^{18}\text{O}$ values. In anoxic conditions, microbial activity can significantly affect $\delta^{34}\text{S}$ without changing $\Delta^{17}\text{O}$ signatures. However, the fact that the Lake Tecopa was a shallow lake (<5 – 10 m; e.g. Larsen 2008) as evidenced by the presence of ripple marks and cross-laminations in the sediments, and the fact that no S-bearing minerals such as pyrite are observed in our samples suggest limited (if any) sulfate biogenic reduction effects on sulfate isotopic values.

In order to explain the $\sim 8\%$ $\delta^{18}\text{O}$ and $\sim 5\%$ $\delta^{34}\text{S}$ ranges measured in sulfate sediments, we suggest mixing of two sources of mass-dependent sediment-derived sulfates (MDSDS): 1) lacustrine or fluvial sulfates ($\delta^{18}\text{O} \sim -2\%$; $\delta^{34}\text{S} \sim 15\%$) and 2) evaporitic sulfates ($\delta^{18}\text{O} \sim 15\%$; $\delta^{34}\text{S} \sim 22\%$).

Lacustrine or fluvial sulfates are formed by aqueous abiotic or biological oxidation of S-bearing minerals. During such process the ambient water is the source of 50% to 100% of the sulfate oxygen depending on the pH or Fe^{3+} concentration (Van Stempvoort and Krouse, 1994). The Lake Tecopa water likely had the same composition as the present day Amargosa river water, $\delta^{18}\text{O} \sim -13\%$, $\delta^{34}\text{S} \sim 15\%$ (Yang et al., 1997; Larsen et al., 2001) and $\Delta^{17}\text{O} \sim 0\%$. The sulfates in equilibrium with

Fig. 3. Stratigraphic section of Lake Tecopa (modified from Hillhouse, 1987) with ash proportion, sulfate $\Delta^{17}\text{O}$, $\delta^{34}\text{S}$, $\delta^{18}\text{O}$ composition, SO_4 and CaCO_3 concentrations, and calculated proportions of the different sulfate sources (MIVS, lacustrine or fluvial MDSDS, evaporitic MDSDS) through the profile (see text for more details). This cumulative section is based on 18 different studied profiles (Fig. 2). The curve that fits the maximum $\Delta^{17}\text{O}$ relates the mass-independent signature of oxygen isotopes through the sedimentary record. Ash proportions were determined under the microscope in the freshest sampling profiles. HRT ash proportion was not determined due to ash alteration into K-feldspar. See the text for more details about the estimation of the atmospheric background ($AB = 0.2\%$; Section 5.1.1) as well as the Fig. 6 for the sedimentary background ($SB = 0.5\%$). Notice that $\Delta^{17}\text{O}$ higher than the SB are systematically correlated to high concentration of ash.

Table 1
Sulfate compositions of Lake Tecopa ash layers and sediments.

Samples	Height (m)	SO ₄ (ppm)	CaCO ₃	Δ ¹⁷ O	δ ¹⁸ O	δ ³⁴ S	MIVS	MDSDS 1	MDSDS 2	Total
1LCT + 4	4.3	211	4	1.95	7.95		0.22	0.65	0.24	1.11
1LCT + 4 *	4.3	211	4	1.78	5.64	15.06				
1LCT + 3	3.6	369	4	0.62	10.01	16.62	0.08	0.20	0.62	0.90
1LCT + 2	2.6	38	4	0.96	8.49	16.87	0.17	0.39	0.18	0.74
1LCT + 1	2.2	88	0	1.55	4.76	14.28	0.19	0.64	0.21	1.05
1LCT8	2.1	365	0	0.92	1.97	15.74	0.11	0.86	0.13	1.10
1LCT8 *		365	0	0.94	4.22					
1LCT7	1.9	33	0	1.36	4.07	12.93	0.17	0.60	0.18	0.95
1LCT6	1.7	32	0	0.78	−0.06	12.30	0.10	0.81	0.01	0.91
1LCT5	1.1	0	0							
1LCT4	1.0	53	0	1.86	4.39	12.67	0.23	0.63	0.14	1.01
1LCT3	0.7	117	0	1.79	3.04	12.83	0.22	0.74	0.08	1.04
1LCT2	0.4	0	0							
1LCT1	0.1	40	0	0.37	8.32					
1LCT − 1	−0.1	123	3	0.80	3.60	15.90	0.10	0.72	0.23	1.05
1LCT − 2	−0.6	252	4	0.64	2.85					
1LCT − 3	−1.7	82	3	0.51	6.57	16.72	0.06	0.47	0.44	0.97
2LCT + 4	5.0	482	2	0.52	6.48					
2LCT + 3	4.6		4							
2LCT + 2	4.0		4							
2LCT + 1	3.0	107	0	1.19	5.73					
2LCT8	2.7		0							
2LCT7	2.4		0							
2LCT6	2.1		1							
2LCT5	1.8		0							
2LCT4	1.4		1							
2LCT3	1.1	68	0							
2LCT2	0.8		1							
2LCT1	0.3		0							
2LCT − 1	−0.3	21	4							
2LCT − 2	−0.5	45	4	0.43	6.76					
3LCT2	0.8	133	0	0.51	3.83					
3LCT1	0.0	107	0	0.58	7.55					
4LCT3	2.0	267	1	1.38	7.80					
4LCT3 *				1.15	6.69					
4LCT2	1.0	281	1	0.35	9.44					
4LCT2 *				0.25	6.81					
4LCT1	0.0	286	0	0.18	7.91					
6LCT2	0.5	16	1	1.04	9.35	16.39	0.13	0.31	0.53	0.97
6LCT1	0.0	9	0	1.66	9.25					
7LCT2	0.6	21	0	0.05	10.18					
7LCT1	0.0	215	0	0.21	5.64					
8LCT1	0.1	85	4	0.56	7.09					
9LCT1	0.1	39	4	0.49	7.49					
9LCT1 *				0.21	6.53					
10LCT1	0.3	25	0	1.94	8.54	16.16	0.24	0.50	0.39	1.14
IBO4 − 4 ^a	2.5	610		2.26	5.97	7.8				
IBO4 − 3 ^a	0.2	290		2.05	12.11	6.1				
IBO4 − 1 ^a	2.5	240		1.56	8.8	9.2				
1BT + 2	1.6	507	3	0.61	9.63					
1BT + 2*		507	3	0.48	7.70					
1BT + 1	0.8	712	2	0.28	6.29					
1BT + 1*				0.31	5.71					
1BT4	0.8	2282	3	0.31	10.21					
1BT4*				0.30	4.81					
1BT3	0.5	305	1	0.26	5.15					
1BT2	0.3	221	0	0.33	5.15					
1BT2*				0.14	5.69					
1BT1	0.0	359	0	0.36	5.56					
2BT + 3	4.5	662	3	0.29	3.12					
2BT + 2	2.5	518	4	0.27	3.73	16.19	0.03	0.64	0.30	0.97
2BT + 1	1.0	820	4	0.23	4.94					
2BT + 1*				0.21	2.51					
2BT4	0.7	96	3	0.28	8.79	18.15	0.04	0.34	0.60	0.97
2BT3	0.4	66	3	0.34	7.36					
2BT2	0.2		1							
2BT1	0.1	53	1	0.99	7.02	16.27	0.12	0.49	0.41	1.02
2BT − 1	−0.1	7	0							
2BT − 2	−0.4	115	1	0.15	8.86	17.12	0.02	0.25	0.61	0.88
2BT − 3	−1.0		3							
3BT1	0.5	291	1	1.48	5.48	14.80	0.18	0.60	0.26	1.05
3BT1*		291	1	1.25	3.21					
4BT2	2.6	249	1	0.67	7.53					
4BT1	0.1	188	1	0.30	6.19					
4BT1*				0.29	7.55					
5BT1	0.1	8	0							

Table 1 (continued)

Samples	Height (m)	SO ₄ (ppm)	CaCO ₃	Δ ¹⁷ O	δ ¹⁸ O	δ ³⁴ S	MIVS	MDSDS 1	MDSDS 2	Total
6BT1	0.1	139	1	0.12	7.20					
12BT2	2.0	368	0	0.00	3.88					
12BT2*		368	0	0.08	3.96					
12BT1	0.0	158	0	0.23	6.41					
IBO4 – 6 ^a	0.1	2720		0.66	4.1	12.5				
1HRT3	0.4	178	2	0.19	3.83					
1HRT2	0.1	164	1	0.13	5.21					
1HRT2*				0.33	5.82					
1HRT1	0.01	161	1	0.06	5.17					
2HRT + 2	1.4	516	3	0.75	7.60	19.72				
2HRT + 2*		516	3	0.40	6.59		0.05	0.62	0.47	1.14
2HRT + 1	0.7	5772	3	0.30	6.08					
2HRT2	0.35	181	2	0.59	6.84	17.64	0.07	0.51	0.45	1.04
2HRT1	0.05	62	2	0.75	9.30	18.06	0.09	0.36	0.57	1.03
2HRT – 1	–0.2	10	1							
2HRT – 2	–0.6	3627	2	0.39	7.14	18.83	0.05	0.53	0.50	1.07
2HRT – 2*				0.29	6.59					
2HRT – 3	–1	668	1	0.42	7.45					
IBO4 – 8 ^a	0.2	1360		0.76	8.54	19.8				
									Average	1.01
									Std dev	0.09
Other localities :										
Toba (74 ka)		<5								
JD – 1		16		0.42	10.65					
JD – 4		91		0.03	1.93					
JD – 2		205		0.10	12.24					

LCT: Lava Creek Tuff; BT: Bishop Tuff; HRT: Huckleberry Ridge Tuff. JD: Ash deposit (28Ma) from the John Day Fossil Beds National Monument.

1LCT1: profile 1 – Lava Creek Tuff ash layer – sample 1. Samples are defined as from above (+) or below (–) ash layers and the height is measured from the bottom of each ash layers. The location of each profile is shown on the Fig. 2.

δ¹⁸O is normalized to SMOW (standard mean ocean water) and δ³⁴S to CDT (Canyon Diablo Triolite).

SO₄ concentration was estimated from the proportion of BaSO₄ (containing 41 wt.% SO₄) precipitated from the leaching solution of each sample. CaCO₃ concentration was estimated by qualitative reaction of sample in contact with concentrated HCl (arbitrary scale from 0–no reaction to 4–violent reaction).

Sulfate source proportions: MIVS = Mass-independent volcanic sulfate; MDSDS 1 = Mass dependent sediment-derived sulfate (lacustrine or fluvial in origin); MDSDS 2 = Mass-dependent sediment-derived sulfate (evaporitic in origin).

*Barite was purified via the DTPA dissolution–reprecipitation treatment (for more details, see the supplementary material).

^a Data from (Bindeman et al., 2007).

this water would have a low δ¹⁸O (~–2‰), δ³⁴S ~ 15‰ and Δ¹⁷O ~ 0–0.2‰ (Fig. 5). Evaporitic sulfate are also generated by aqueous oxidation of S-compounds, however in this case, water evaporation induces isotopic fractionation, leading to the concentration of the heaviest isotopes. This is supported by the measurements performed in salt from Lake Tecopa δ¹⁸O ~ 15‰, δ³⁴S ~ 22‰ and Δ¹⁷O ~ 0‰ (e.g. Bindeman et al., 2007). Sulfate derived from the dissolution of old evaporitic deposits is also a possibility.

Another mass-dependent sulfate source that can provide long-term contribution is mass-dependent volcanic sulfates (MDVS). They are usually delivered by small eruptions that release SO₂ that is

oxidized by mass-dependent pathways during atmospheric transport. The MDVS may have a composition close to the tropospheric processed sulfate precipitated in volcanic plumes, close to the eruption center with Δ¹⁷O ~ 0‰, δ¹⁸O ~ 6‰ and δ³⁴S ~ 6–8‰ as measured in different studies (Luhr and Logan, 2002; Bao and Reheis, 2003; Bindeman et al., 2007; Mather et al., 2007).

5.1.3. Mixing model

Fig. 5 shows Δ¹⁷O vs. δ¹⁸O and Δ¹⁷O vs. δ³⁴S correlations, where these sulfate source end-members are plotted. Data is fitted with an ash-

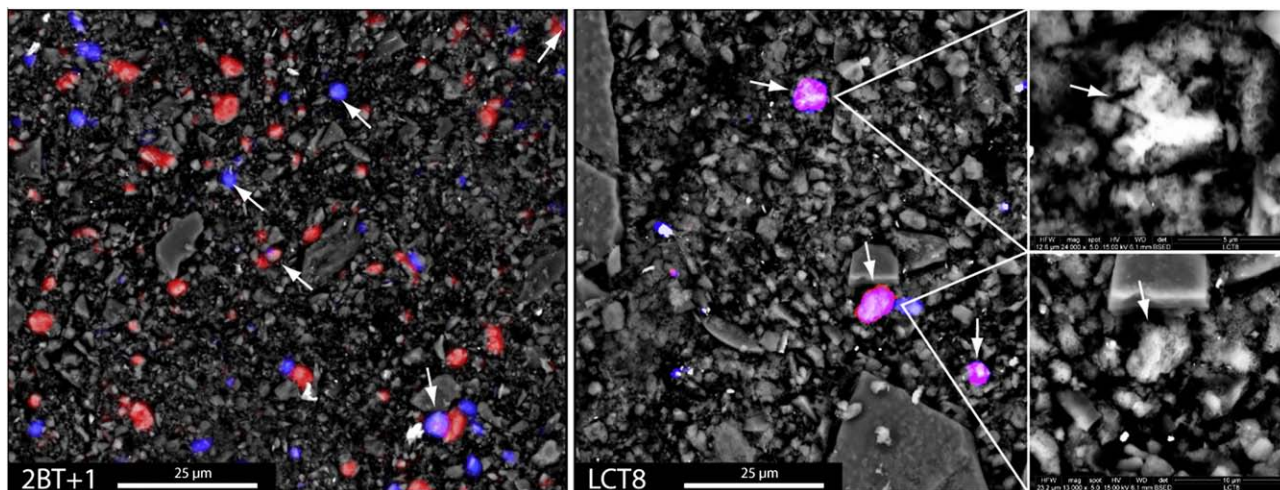


Fig. 4. SEM images and X-ray mapping (current of 15 kV and 2 nA) of sediment (2BT + 1) and ash (LCT8) samples. Ca concentration is in red and S concentration in blue. The arrows show where Ca and S maps overlap indicating the presence of CaCO₃ crystals aggregates (gypsum or anhydrite).

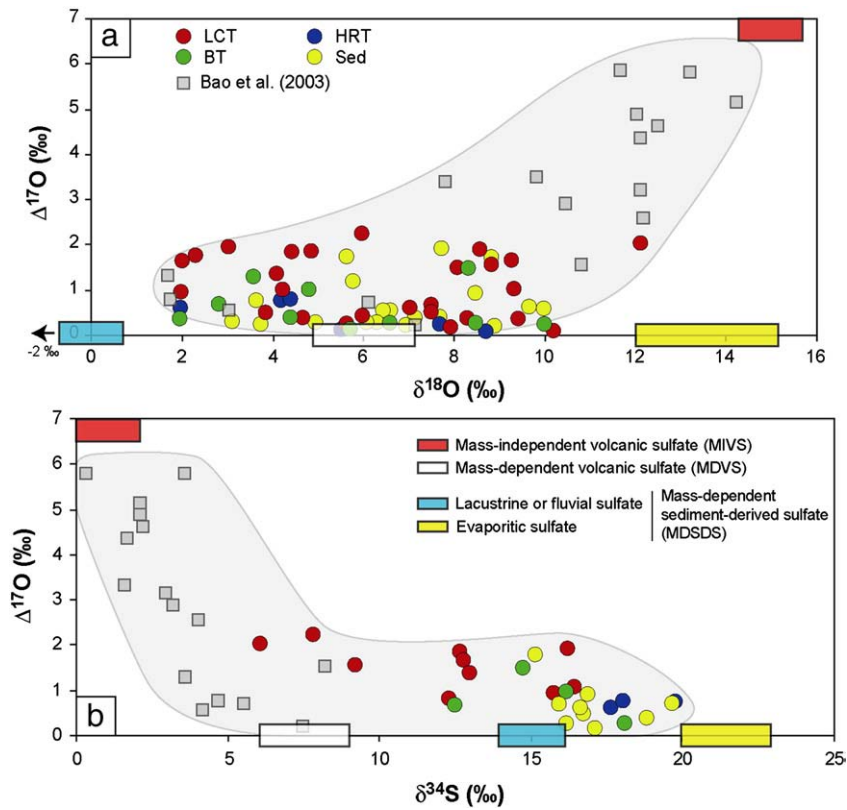


Fig. 5. Isotopic correlation of $\Delta^{17}\text{O}$ with (a) $\delta^{18}\text{O}$ and (b) $\delta^{34}\text{S}$ measured in sulfate from ash layers and enclosing sediments of Lake Tecopa. The composition ranges are interpreted to represent mixing of MIVS and MDSDS. Sulfate analyses from an ash bed in Nebraska (USA) resulting from an unknown supereruption are plotted (Bao et al., 2003) for comparison and extend trends from this study. See the text for details on sulfate source compositions.

sediment mixing model, which determines their relative contribution in each of our samples. As the main interest of this study is to trace MIVS signature, the proposed mixing model consists of MIVS and two MDSDS end-members. In order to calibrate the robustness of the linear model, several different combinations of potential isotopic values of end-member sulfate sources were tested. The isotopic composition of the end-members that best fit our data have the following composition: MIVS: $\delta^{18}\text{O} = 15\text{‰}$, $\delta^{34}\text{S} = 0\text{‰}$ and $\Delta^{17}\text{O} = 8\text{‰}$ and MDSDS: lacustrine or fluvial: $\delta^{18}\text{O} = -2\text{‰}$, $\delta^{34}\text{S} = 15\text{‰}$ and $\Delta^{17}\text{O} = 0\text{‰}$ and evaporitic: $\delta^{18}\text{O} = 20\text{‰}$, $\delta^{34}\text{S} = 12\text{‰}$ and $\Delta^{17}\text{O} = 0\text{‰}$. The relative participation of each end-member in our samples has been evaluated by monitoring the standard deviation of the sums of the three source proportions; such error propagation approach is similar to that proposed by Bao and Marchant (2006). However, if other computed mixing models are performed with $\delta^{18}\text{O}$ and $\delta^{34}\text{S}$ 2–3‰ and $\Delta^{17}\text{O}$ 0.2–0.3‰

isotopically-different end-members, similar conclusions are drawn from our dataset.

The calculated proportions of MIVS yield 23% in LCT, 18% in BT and 9% in HRT, decreasing with age (Table 1 and Fig. 3). There is no evidence supporting that the far larger (2500 km³), HRT, eruption initially contained less MIVS than the 1000 km³ LCT or the 750 km³ BT. Rather, we interpret its lower MIVS contents as resulting from greater dilution of HRT sulfate by MDSDS with time.

This mixing model demonstrates that the main source (>77%; Table 1) of sulfate in the Lake Tecopa stratigraphic record is mass-dependent sedimentary sulfate (MDSDS). Assuming a more-or-less constant isotopic composition of the sedimentary sulfate sources with time, the fluctuations between “lacustrine or fluvial” and “evaporitic” sources could reveal the oscillating lake's depth history. The proportion of MDSDS in sediments least affected by ash leachates reaches

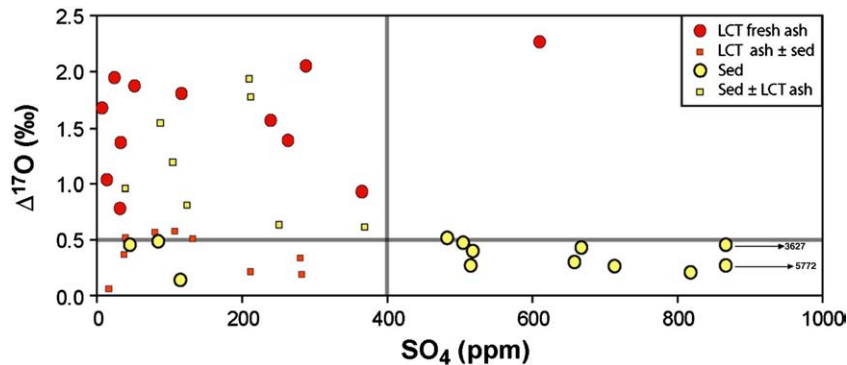


Fig. 6. Scattered negative correlation of $\Delta^{17}\text{O}$ vs. SO_4 concentration in LCT deposit and enclosing sediments, demonstrating $\Delta^{17}\text{O} > 0.5\text{‰}$ and most likely sulfate concentration <400 ppm values for ash sulfate and $\Delta^{17}\text{O} < 0.5\text{‰}$ and usually sulfate concentration >400 ppm for sediment sulfate. Contamination of ash by sediment tends to decrease the overall sulfate $\Delta^{17}\text{O}$ (<0.5‰) whereas the opposite is observed for the contamination of sediment by ash ($\Delta^{17}\text{O} > 1\text{‰}$). Therefore, the $\Delta^{17}\text{O} = 0.5\text{‰}$ line corresponds to the maximum sediment background (SB in Fig. 3).

98%, while the ash layer themselves are quite diluted and contain between 77% and 93% of MDSDS (Table 1), which represent between 15 and 45 ppm of MIVS remaining in ash layers.

5.1.4. Preservation of $\Delta^{17}\text{O}$ signal in sulfate

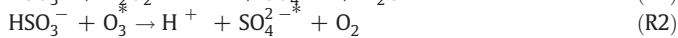
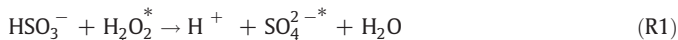
In the case of complete sediment-ash sulfate mixing, one would expect homogeneous sulfate concentrations, and isotopic values, through the sedimentary record. Higher sulfate concentration in sediment than ash (Table 1 and Fig. 6) indicates that sulfates from ash and sediment are not fully mixed. Thus, one major result of the mixing model, is the demonstration that although heavily diluted, the MIVS is preserved in ash beds from Lake Tecopa for hundreds of thousands to few million years. The proportion of MIVS in ash layers (and $\Delta^{17}\text{O}$ signature) decays with age and/or thickness of the volcanic deposits from LCT through BT to the HRT ash layer (Fig. 3). Consequently, the $\Delta^{17}\text{O}$ signal decays in the geologic record can be quantified using our three data points (LCT, BT and HRT) with a hypothetical modern “super-volcanic” ash deposit with undiluted 100% MIVS with $\Delta^{17}\text{O} = 8\%$. In this quantification, it is assumed that the modern supereruption and ash deposition happened 10 years ago, and was followed by continuous acid precipitations. We observe that the best fit parameter of dilution of MIVS by MDSDS is expressed by a logarithmic function $y = -7.26\ln(x) + 16.6$; $R^2 = 0.99$ ($x = \text{time}$ and $y = \text{MIVS proportion}$).

This equation shows that after 5 Ma, the MIVS signal becomes completely blended with the MDSDS leading to an average $\Delta^{17}\text{O} < 0.5\%$, which is indistinguishable from that of the sedimentary background measured in Lake Tecopa. Note that in a sedimentary record where the ash layer proportion is significant (e.g. 15–20% in Lake Tecopa), the sedimentary background can also significantly increase with time. These estimations are consistent with $\Delta^{17}\text{O} < 0.42\%$ that we measured in sulfates from the 28 Ma ash layer from an unknown supereruption in the arid environment of John Day Fossil Beds National Monument in central Oregon (Table 1). In this regard, the preservation of $\Delta^{17}\text{O}$ up to 5.84‰ in volcanic sulfate from the 28 Ma old deposit in Nebraska (USA, Bao et al., 2003) deserves discussion and comparison with sediments from Lake Tecopa. In Nebraska, volcanic mass-independent sulfate occurs as admixture to carbonate cement. This secondary carbonate forms pseudomorphs over gypsum rosettes (Bao and Reheis, 2003; Bao, 2005). It appears that this high ^{17}O -excess (5.84‰) could only be preserved in such an old deposit (28 Ma) because soon after the gypsum formation it was encapsulated into the carbonate. In Lake Tecopa, as expected for most of the ash deposits in the world, MIVS is preserved as original volcanic gypsum particle aggregates between glass shards (Fig. 4). Our decay modeling indicates that gypsiferous cement environments are less stable hosts for MIVS.

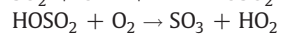
5.2. Formation of ^{17}O -excess in volcanic sulfates

We next address the origin of $\Delta^{17}\text{O}$ signature in MIVS. The three main oxidation pathways of volcanic SO_2 into oxygen mass-independent sulfates are as follow (with * indicating the ^{17}O -excess):

Heterogeneous aqueous phase oxidation:



and homogeneous gas phase oxidation (e.g. Seinfeld and Pandis, 1998 and references therein):



It is important to note that the reaction R1 and R2 take place in the troposphere and not in the stratosphere, which is water-poor. However, reaction R3 takes place in both the troposphere and stratosphere, but it

is only able to transfer the ^{17}O -excess to the sulfates generated in the stratosphere. Indeed, in the troposphere, the rapid isotopic exchange between the mass-dependent water and OH^* leads to rapid loss of the initial ^{17}O -excess of the OH^* radicals (e.g. Lyons, 2001).

In the troposphere, the oxidation of mass-dependent volcanic SO_2 can also be achieved by reaction with hydrogen peroxide (H_2O_2^* ; R1). In this case 1/2 of the oxygen atoms contained in sulfates are coming from H_2O_2^* . Typically hydrogen peroxide has $\Delta^{17}\text{O} \sim 2\%$ (Savarino and Thiemens, 1999), which implies that the MIVS will only have $\Delta^{17}\text{O} < 1\%$. Most of the $\Delta^{17}\text{O}$ recorded in the Lake Tecopa ash layers are greater than 1‰ and the computed original MIVS $\Delta^{17}\text{O}$ is as high as 8‰, precluding an important role played by the H_2O_2^* oxidation pathway (R1). This also leads to the conclusion that the ozone oxidation pathways (R2 and/or R3) play a major role in the formation of MIVS. On average, the atmospheric ozone, which is 90% stratospheric, has an average $\Delta^{17}\text{O}$ value of 32‰ and a high $\delta^{18}\text{O}$ value up to 100–150‰ (e.g. Krankowsky et al., 2000). If OH^* radicals possess the same $\Delta^{17}\text{O}$ as their ozone precursors during photodissociation, SO_2 oxidation into MIVS inherits 1/4 of the oxygen atoms from the mass-independent O_3^* (R2) or OH^* radicals (R3) leading to $\Delta^{17}\text{O}$ of about 8‰ (e.g. Thiemens, 2006). High $\delta^{18}\text{O}$ ($\sim 15\%$) and low $\delta^{34}\text{S}$ ($\sim 0\%$) are also expected for MIVS as deduced from the correlation between these isotopic ratios and $\Delta^{17}\text{O}$ (Fig. 5). It appears from Bao et al. (2003) and our dataset that the processed high $\Delta^{17}\text{O}$ sulfates are lighter in terms of S-isotopes than the initial volcanic SO_2 .

5.3. Incorporation of MIVS in ash layers, and surface dynamics of its accumulation in sediment basins

Supereruptions release $\geq 10^3 \text{ km}^3$ of ash and $> 10^3$ megatons of SO_2 into the atmosphere (e.g. Wallace, 2001). Although by air-fall deposition ash blankets wide areas after a few days to a few weeks (e.g. HRT: $\sim 3.10^6 \text{ km}^2$; Toba (74 kyr): $\geq 5.10^6 \text{ km}^2$), ice core records from Antarctica show that the oxidation of SO_2 gas to SO_3 and H_2SO_4 aerosols requires months to years (e.g. Zielinski et al., 1996). Thus MIVS can fall as sulfuric acid precipitation: wet (acid rain), or dry (e.g. “dry fogs”). Then, it is incorporated into ash-covered ground and forms gypsum (Fig. 4), months to years after the ash deposition itself. Calculations suggest that MIVS concentration of 50ppm are possible if the majority of sulfuric acid precipitation occurs in $\sim 5000 \text{ km}$ radius from the supervolcano, due to atmospheric circulation (e.g. cyclonic current) that is able to concentrate aerosols clouds in the upper troposphere and lower stratosphere as observed with smaller-scale eruptions (e.g. Rose et al., 2001). In order to account for the meter-thick deposits in Lake Tecopa and similar basins elsewhere, local fluvial and/or eolian redistribution of ash (and sulfate) from the watershed area is required (e.g. Rose et al., 2003). Then, as observed for each outcrop, prolonged intra-basin lacustrine and fluvial reworking of sediment and ash (and sulfate) occurs.

5.4. Mass independent $\Delta^{33}\text{S}$ and $\Delta^{36}\text{S}$

Our detailed isotopic dataset for ash in Lake Tecopa permits discussion on rare sulfur isotopes fractionation after large vs. small volcanic eruptions, and comparison with sulfate in Antarctic ice. The latter shows mass-independent $\Delta^{33}\text{S}$ of -0.5% to 1.16% and $\Delta^{36}\text{S}$ of -2.70% to 1.98% (Savarino et al., 2003b; Baroni et al., 2008; Fig. 7), but only small $\Delta^{33}\text{S}$ (-0.03% to -0.07%) and $\Delta^{36}\text{S}$ ($+0.03\%$ to $+0.28\%$) values were previously reported in Lake Tecopa LCT and BT ash beds (Bindeman et al., 2007; Fig. 7). Because these values were small, they were earlier interpreted to reflect mass-dependent processing by kinetic gas phase reaction and/or Rayleigh distillation involving a residual Rayleigh reactant (Bindeman et al., 2007). Since significant $\Delta^{33}\text{S}$ and $\Delta^{36}\text{S}$ have not been measured in sulfate from small eruption deposits (Bindeman et al., 2007; Fig. 7), we need to

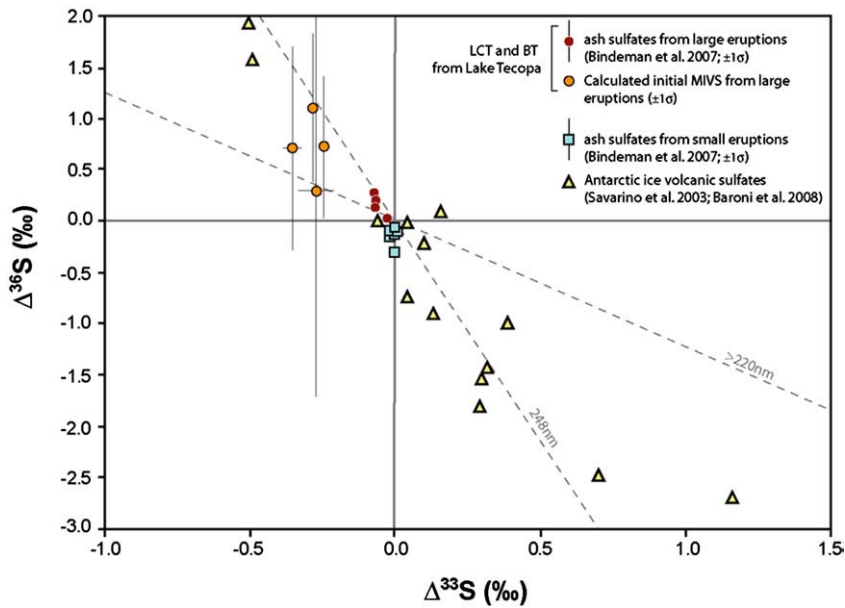


Fig. 7. Compilation of $\Delta^{33}\text{S}$ and $\Delta^{36}\text{S}$ measured in volcanic sulfates. Ash-sulfates from large and small eruptions are from Bindeman et al. (2007) and Antarctica ice volcanic sulfates are from Savarino et al. (2003b) and Baroni et al. (2008). The initial isotopic values for MIVS from LCT and BT deposits from Lake Tecopa were calculated using the proportion of dilution by MDSDS (see text for more details). Isotopic fractionation of SO_2 photolysis experiments at different wavelengths are plotted (Farquhar et al., 2001) and indicate that SO_2 photolysis during volcanic eruption took place under UV radiation between 220 and 248 nm, likely in the upper stratosphere. Only large eruptions ($> 600 \text{ km}^3$) show mass-independent sulfates in ash deposits, whereas small eruptions ($< 600 \text{ km}^3$) show sulfate mass-independent behavior. Antarctic ice sulfates record exclusively stratospheric aerosols with extreme mass-independent signatures. The error bars for the “initial MIVS from large eruptions” are propagated errors in 1σ (between 0.7 and 2.0‰ for $\Delta^{36}\text{S}$ and between 0.02 and 0.06‰ for $\Delta^{33}\text{S}$) from the analytical uncertainties determined on the “ash sulfates from large eruptions” ($\Delta^{36}\text{S} \pm 0.2$ and $\Delta^{33}\text{S} \pm 0.006$; Bindeman et al., 2007).

find a process able to explain the significant mass-independent $\Delta^{33}\text{S}$ and $\Delta^{36}\text{S}$ signatures characteristic of sulfate from large eruptions.

Here, we discuss a process able to explain these small but significant $\Delta^{33}\text{S}$ and $\Delta^{36}\text{S}$ values measured in sulfate from LCT and BT-samples from Lake Tecopa. The linear mixing model above suggests that MIVS constitutes 20–28% of LCT and 10% of the BT sulfates in these samples. Assuming that MIVS was diluted by MDSDS with $\Delta^{33}\text{S} = 0\text{‰}$ and $\Delta^{36}\text{S} = 0\text{‰}$, we obtain initial undiluted MIVS values of $\Delta^{33}\text{S} = -0.24\text{‰}$ to -0.35‰ and $\Delta^{36}\text{S} = 0.27\text{‰}$ to 1.08‰ (Fig. 7). When plotted together with data for the stratospheric sulfate from Antarctica ice, the estimated MIVS compositions from Lake Tecopa ash extends the negative correlation trend, and plot between photolytic wavelengths of 220–248 nm (e.g. Farquhar et al., 2001). This suggests a common photolytic mechanism for both, but also suggest that sulfates in ash layers and in Antarctica ice are generated by different timescales and processes. We propose that ash-sulfates are quickly generated and removed from the stratosphere by ash sedimentation and acid precipitations. Pavlov et al. (2005) modeled that volcanic sulfates generated by photolysis of SO_3 have initially small negative $\Delta^{33}\text{S}$ that later becomes positive. However, Baroni et al. (2007) measured in volcanic sulfate deposited in Antarctica large positive $\Delta^{33}\text{S}$ values that become negative due to mass-balance effects.

We conclude that sulfate in ash layers most likely record isotopic values of the first volcanic sulfate removed from the atmosphere, with small and negative $\Delta^{33}\text{S}$ as inferred from the Pavlov et al. (2005) model. On the other hand, ice cores record the volcanic sulfate generated after a long journey in the stratosphere, leading to large mass-independent $\Delta^{33}\text{S}$ signatures due to long UV radiation exposure as observed in Baroni et al. (2007).

5.5. Climatic impact of supereruptions

The chemical and physical state of the atmosphere after super-volcanic eruptions is a matter of considerable debate and extrapolative modeling (e.g. Robock, 2004). The large ^{17}O -excesses measured in the Lake Tecopa sulfate indicate atmospheric reaction

with ozone or O_3 -derived compounds to make H_2SO_4 (reactions R2 and R3) and this process is able to consume ozone and water; thus we discuss the possibility of atmosphere hydration or dehydration and ozone depletion.

5.5.1. Stratosphere hydration or dehydration: implications on MIVS formation

The SO_2 oxidation by OH^* radical produces highly hydroscopic SO_3^* compounds that quickly react with water to produce H_2SO_4^* (reaction R3). This reaction feeds the discussion on the relative role of volcanic SO_2 in drying out the stratosphere (e.g. Bekki, 1995). However, it is not yet clear how much water is injected into the stratosphere by a major volcanic plume. The generalization of stratospheric “watering”, as observed after the 1982 El Chichón eruption, is still under debate (e.g. Shepherd, 2002; Robock, 2004).

The hydration/dehydration balance after a supereruption may be mostly controlled by the physical state of the tropopause. The tropopause is characterized by a sharp decrease of atmospheric temperature, which normally prevents water transfer from the troposphere to the stratosphere. After large volcanic eruptions, the tropopause, contaminated by sulfate aerosol clouds, is heated up by absorption of the incoming solar radiation (e.g. Robock, 2000), a process able to increase the water flux from the troposphere to the stratosphere (e.g. Joshi and Shine, 2003). As a result, an important consequence of the stratosphere hydration after a supereruption is that due to faster reaction rates (Seinfeld and Pandis, 1998), heterogeneous oxidation reactions R1 and/or R2 play a more important role. Therefore, in a “hydrous” stratosphere, the ozone mass-independent signature would be transferred to volcanic sulfate aerosols more efficiently by the direct SO_2 oxidation via O_3^* (R2) rather than by OH^* radicals (R3).

5.5.2. Ozone consumption

In either process of stratospheric dehydration or hydration, ozone molecules are consumed during the oxidation of volcanic SO_2 . In 1991, the 10 km^3 eruption of Pinatubo released $\sim 20 \text{ Mt}$ SO_2 and resulted in

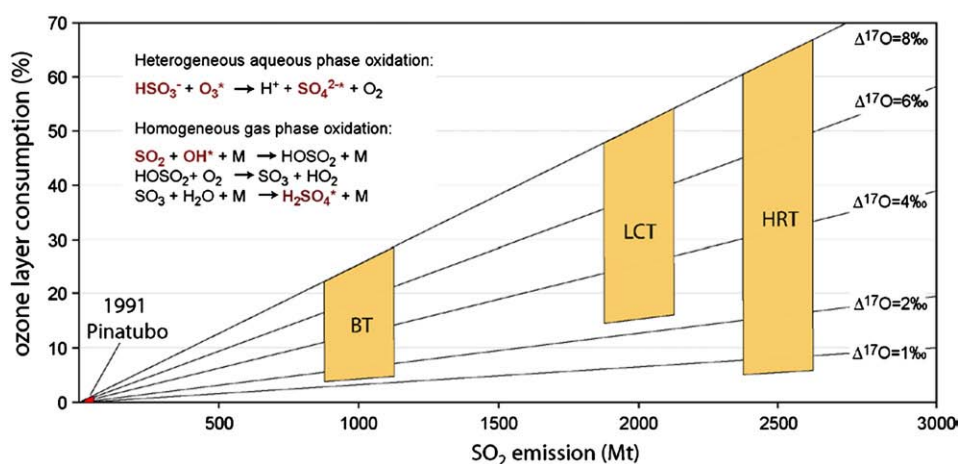


Fig. 8. Estimation of the ozone layer consumption by the volcanic SO_2 oxidation into sulfates as a function of the volume of SO_2 released by supereruptions and $\Delta^{17}\text{O}$ measured in sulfates from volcanic deposits. Volcanic SO_2 emissions are scaled to the erupted magma volumes (Wallace, 2001). The proportion of the ozone layer consumed is calculated relatively to the present day ozone layer concentration (300 DU (Dobson Unit) or 6.85×10^{13} mol globally). The gray boxes show the ozone consumption ranges estimated for the three studied supereruptions as well as 1991 Pinatubo eruption. The minimum values are based on maximum $\Delta^{17}\text{O}$ measured in the sulfate from this study, while maximum values are based on $\Delta^{17}\text{O} = 8\text{‰}$, estimated for the primary volcanic sulfate (see text). Notice that a supereruption like HRT, 250 times larger than the 1991 Pinatubo eruption is potentially capable to destroy 50% of the whole ozone layer.

an ozone layer depletion of 3–4%, directly attributable to the eruption (Gleason et al., 1993; McCormick et al., 1995). The ozone layer consumption would be much more dramatic after LCT, BT and HRT supereruptions that released 75 to 250 times more SO_2 .

The ozone concentration stays approximately constant due to the balance between formation and destruction processes (e.g. Seinfeld and Pandis, 1998). During and shortly after a supereruption, the atmosphere will not be able to counterbalance the ozone depletion due to volcanic aerosol formation. The oxidation of massive amounts of volcanic SO_2 that leads to MIVS can consume ozone indirectly (R2) or directly (R3), leading to temporal decrease of global ozone concentration. When the volume of volcanic SO_2 released by an eruption and the $\Delta^{17}\text{O}$ measured in sulfate from the ash deposit are considered together, it is possible to estimate the mass of ozone consumed by the reactions R1 and R3 (Fig. 8): 5–25% after the BT eruption, 15–50% after LCT eruption, and between 6–65% after the HRT eruption. As SO_2 concentration is likely to be heterogeneously dispersed in the atmosphere, the overall ozone depletion may be greater in the northern hemisphere or at some specific latitudes depending on the atmospheric circulation. These are most likely minimal estimates, since for the Pinatubo eruption that emitted 20 Mt SO_2 and generated volcanic sulfate with $\Delta^{17}\text{O}$ up to 4.7‰ (from Antarctica ice; Savarino et al., 2003a) our model predicts 0.3 to 0.4% depletion of the global ozone layer (Fig. 8). This is ten times lower than the observed ozone depletions and suggests other compounds besides SO_2 such as anthropogenically-produced chlorine (Solomon et al., 1993) played an important role. Other volcanic compounds such as HCl (e.g. McCormick et al., 1995) and abundant aerosol surface particles may additionally contribute to the ozone layer depletion after supereruptions due to acceleration of heterogeneous surface reactions.

As the SO_2 is capable of absorbing short wavelength UV radiation (Finlayson-Pitts and Pitts, 2000), therefore prior its oxidation into sulfate it protects the Earth surface while the ozone production is decreased. Nonetheless, depending on the atmospheric circulation, heterogeneous distribution of SO_2 may lead to local ozone holes and direct exposure of the Earth surface to short wavelength UV radiations; and these consequences would be of prime importance for life on the Earth.

5.5.3. Tropospheric vs. stratospheric sulfate transport during supereruptions

Due to remoteness of Lake Tecopa (Fig. 1), and the fact that atmospheric precipitation of MIVS occurred in a ~5000km radius from

the eruptive centers, stratospheric jet stream transport of ash and aerosols is obviously required.

Moreover, this study shows that up to 20–60% of global ozone could be consumed after supereruptions. As only 10% of the ozone is tropospheric, consumption of at least 10% of the stratospheric ozone and generation of stratospheric MIVS is required.

Confirmation of the mass-independent signature of S-isotopes in LCT and BT sulfate indicates a volcanic SO_2 photolysis in the upper stratosphere, unless a local ozone hole created by a supereruption permits SO_2 photolysis at lower altitudes.

The preceding discussion leads to the conclusion that mass-independent signatures of volcanic sulfates from supereruptions have features of both tropospheric and stratospheric transport. This may not necessarily be mutually exclusive and reflect physical degradation by temperature increase and chemical degradation by ozone-depleting reactions of the tropopause. We can speculate that the physical and chemical distinction between high-troposphere and low-stratosphere, at least on a local scale, is erased by supereruptions.

Acknowledgement

We thank Jay Kaufman for the S-isotopes measurement at the University of Maryland, Eloïse Gaillou for her assistance on the SEM and Jeff Post for the X-ray diffraction analyses at the Smithsonian Institution, and Craig Chesner for sharing his Toba samples. We are grateful to Hervé Martin and Kathryn Watts for thoughtful comments on an early draft of the manuscript. Constructive comments from Huiming Bao, James Farquhar and an anonymous reviewer helped to considerably improve this manuscript. Finally, we would thank Marli Miller and Darrel Cowan for their accommodation at Shoshone during the field work. This research project was supported by NSF (EAR-0844772) and PRF (46262-G2).

Appendix A. Supplementary data

Supplementary data associated with this article can be found, in the online version, at doi:10.1016/j.epsl.2009.03.005.

References

- Bao, H., 2005. Sulfate in modern playa settings and in ash beds in hyperarid deserts: implication for the origin of ^{17}O -anomalous sulfate in an Oligocene ash bed. *Chem. Geol.* 214, 127–134.

- Bao, H., 2006. Purifying barite for oxygen isotope measurement by dissolution and reprecipitation in a chelating solution. *Anal. Chem.* 78, 304–309.
- Bao, H., Marchant, K.M., 2006. Quantifying sulfate components and their variations in soils of the McMurdo Dry Valleys, Antarctica. *J. Geophys. Res.-Atmos.* 111, D16301.
- Bao, H., Reheis, M.C., 2003. Multiple oxygen and sulfur isotopic analyses on water-soluble sulfate in bulk atmospheric deposition from the southwestern United States. *J. Geophys. Res.-Atmosphere* 108.
- Bao, H., Thiemens, M.H., 2000. Generation of O₂ from BaSO₄ using a CO₂-laser fluorination system for simultaneous analysis of d18O and d17O. *Anal. Chem.* 72, 4029–4032.
- Bao, H., Michalski, G.M., Thiemens, M.H., 2001. Sulfate oxygen-17 anomalies in desert varnishes. *Geochim. Cosmochim.* 65, 2029–2036.
- Bao, H., Thiemens, M.H., Loope, D.B., Yuan, X.L., 2003. Sulfate oxygen-17 anomaly in an Oligocene ash bed in mid-North America: was it the dry fogs? *Geophys. Res. Lett.* 30, 11–14.
- Baroni, M., Savarino, J., Cole-Dai, J.H., Rai, V.K., Thiemens, M.H., 2008. Anomalous sulfur isotope compositions of volcanic sulfate over the last millennium in Antarctic ice cores. *J. Geophys. Res. - Atmosphere.* 113. doi:10.1029/2008JD010185.
- Baroni, M., Thiemens, M.H., Delmas, R.J., Savarino, J., 2007. Mass-independent sulfur isotopic compositions in stratospheric volcanic eruptions. *Science* 315, 84–87.
- Bekki, S., 1995. Oxidation of volcanic SO₂: a sink for stratospheric OH and H₂O. *Geophys. Res. Lett.* 22, 913–916.
- Bindeman, I.N., Eiler, J.M., Wing, B.A., Farquhar, J., 2007. Rare sulfur and triple oxygen isotope geochemistry of volcanogenic sulfate aerosols. *Geochim. Cosmochim.* 71, 2326–2343.
- Blong, R.J., 1984. Volcanic hazards. A sourcebook on the effects of eruptions. Academic Press, Orlando.
- Dorn, R., 1998. Developments in Earth surface processes 6: Rock coating. Elsevier, Amsterdam. 429pp.
- Farquhar, J., Savarino, J., Airieau, S., Thiemens, M.H., 2001. Observation of wavelength-sensitive mass-independent sulfur isotope effects during SO₂ photolysis: implications for the early atmosphere. *Geophys. Res.* 106, 32829–32839.
- Farquhar, J., Savarino, J., Jackson, T.L., Thiemens, M.H., 2000. Evidence of atmospheric sulphur in the martian regolith from sulphur isotopes in meteorites. *Nature* 404, 50–52.
- Farquhar, J., Wing, B.A., 2003. Multiple sulfur isotopes and the evolution of the atmosphere. *Earth Planet. Sci. Lett.* 213, 1–13.
- Finlayson-Pitts, B.J., Pitts, J.N., 2000. Chemistry of the upper and lower atmosphere: Theory, Experiments, and Applications. Academic Press, San Diego. 969 pp.
- Gleason, J.F., Bhartia, P.K., Herman, J.R., McPeters, R., Newman, P., Stolarski, R.S., Flynn, L., Labow, G., Larko, D., Sefort, C., Wellemeyer, C., Komhyr, W.D., Miller, A.J., Planet, W., 1993. Record low global ozone in 1992. *Science* 260, 523–526.
- Hillhouse, J.W., 1987. Late Tertiary and Quaternary geology of the Tecopa basin, southeastern California. Miscellaneous Investigations Series – U. S. Geological Survey.
- Joshi, M.M., Shine, K.P., 2003. A GCM study of volcanic eruptions as a cause of increased stratospheric water vapor. *J. Climate* 16, 3525–3534.
- Khademi, H., Mermut, A.R., Krouse, H.R., 1997. Sulfur isotope geochemistry of gypsiferous aridisols from central Iran. *Geoderma* 80, 195–209.
- Krankowsky, D., Lammerzahl, P., Mauersberger, K., 2000. Isotopic measurements of stratospheric ozone. *Geophys. Res. Lett.* 27, 2593–2595.
- Larsen, D., 2008. Revisiting silicate authigenesis in the Pliocene–Pleistocene lake Tecopa beds, southeastern California: depositional and hydrological controls. *Goesphere* 4, 612–639.
- Larsen, D., Swihart, G.H., Xiao, Y., 2001. Hydrochemistry and isotope composition of springs in the Tecopa basin, southeastern California, USA. *Chem. Geol.* 179, 17–35.
- Luhr, J.F., Logan, M.A.V., 2002. Sulfur isotope systematics of the 1982 El Chichón trachyandesite: an ion microprobe study. *Geochim. Cosmochim.* 66, 3303–3316.
- Lyons, J.R., 2001. Mass-independent fractionation of oxygen-containing radicals in the atmosphere. *Geophys. Res. Lett.* 28, 3231–3234.
- Mather, T.A., McCabe, J.R., Rai, V.K., Thiemens, M.H., Pyle, D.M., Heaton, T.H.E., Sloane, H.J., Fern, G.R., 2007. Oxygen and sulfur isotopic composition of volcanic sulfate aerosol at the point of emission. *J. Geophys. Res.* 111. doi:10.1029/2005JD006584.
- McCormick, M.P., Thomason, L.W., Trepte, C.R., 1995. Atmospheric effects of the Mt Pinatubo eruption. *Nature* 373, 399–404.
- Miller, M.F., 2002. Isotopic fractionation and the quantification of 17O anomalies in the oxygen three-isotope system: an appraisal and geochemical significance. *Geochim. Cosmochim.* 66, 1881–1889.
- Morrison, R.B., 1999. Lake Tecopa: Quaternary geology of Tecopa Valley, California, a multimillion-year record and its relevance to the proposed nuclear-waste repository at Yucca Mountain, Nevada. In: Wright, L.A., Troxel, B.W. (Eds.), *Cenozoic Basins of the Death Valley Region: Boulder, Colorado*. Geological Society of America.
- Pack, A., Toulouse, C., Przybilla, R., 2007. Determination of oxygen triple isotope ratios of silicates without cryogenic separation of NF₃ – technique with application to analyses of technical O₂ gas and meteorite classification. *Rapid Commun. Mass Spectrom.* 21, 3721–3728.
- Pavlov, A.A., Mills, M.J., Toon, O.B., 2005. Mystery of the volcanic mass-independent sulfur isotope fractionation signature in the Antarctic ice core. *Geophys. Res. Lett.* 32, L12816.
- Robock, A., 2000. Volcanic eruption and climate. *Rev. Geophys.* 38, 191–219.
- Robock, A., 2004. Climatic impact of volcanic emissions. In: Sparks, R.S.J., Hawkesworth, C.J. (Eds.), *State of the Planet. Geophysical Monograph*, vol. 150. American Geophysical Union, Washington DC.
- Robock, A., Oppenheimer, D.H., 2003. Volcanism and the Earth's Atmosphere. American Geophysical Union, Washington DC. 360 pp.
- Rose, W.I., Riley, C.M., Dartville, S., 2003. Sizes and Shapes of 10-Ma distal fall pyroclasts in the Ogallala Group, Nebraska. *J. Geol.* 111, 115–124.
- Rose, W.I., Bluth, G.J.S., Schneider, D.J., Ernst, G.G.J., Riley, C.M., Henderson, L.J., McGimsey, R.G., 2001. Observation of volcanic clouds in their first few days of atmospheric residence: the 1992 eruption of Crater Peak, Mount Spurr Volcano, Alaska. *J. Geol.* 109, 677–694.
- Rumble III, D., Farquhar, J., Young, E.D., Christensen, C.P., 1997. In situ oxygen isotope analysis with an excimer laser using F₂ and BrF₅ reagents and O₂ gas as analyte. *Geochim. Cosmochim.* 61, 4229–4234.
- Savarino, J., Bekki, S., Cole-Dai, J.H., Thiemens, M.H., 2003a. Evidence from sulfate mass independent oxygen isotopic compositions of dramatic changes in atmospheric oxidation following massive volcanic eruptions. *J. Geophys. Res.-Atmos.* 108. doi:10.1029/2003JD003737.
- Savarino, J., Romero, A., Cole-Dai, J.H., Bekki, S., Thiemens, M.H., 2003b. UV induced mass-independent sulfur isotope fractionation in stratospheric sulfate. *Geophys. Res. Lett.* 30, 2131.
- Savarino, J., Thiemens, M.H., 1999. Analytical procedure to determine both d18O and d17O of H₂O₂ in natural water and first measurements. *Atmos. Environ.* 33, 3683–3690.
- Seinfeld, J.H., Pandis, S.N., 1998. Atmospheric chemistry and physics. Wiley, New York, p. 1326.
- Shepherd, T.G., 2002. Issues in stratosphere-troposphere coupling. *J. Meteorol. Soc. Jpn.* 80, 769–792.
- Sheppard, R.A., Gude, A.J., 1968. Distribution and genesis of authigenic silicate minerals in tuffs of Pleistocene Lake Tecopa, Inyo County, California. United State Geological Survey Professional Paper, vol. 597. 38pp.
- Solomon, S., Sanders, R.W., Garcia, R.R., Keys, J.G., 1993. Increased chlorine dioxide over Antarctica caused by volcanic aerosols from Mount Pinatubo. *Nature* 363, 245–248.
- Strakey, H.C., Blackmon, P.D., 1979. Clay mineralogy of Pleistocene Lake Tecopa, Inyo County, California. United State Geological Survey Professional Paper, vol. 1061. 34pp.
- Thiemens, M.H., 2006. History and applications of mass-independent isotope effects. *Annu. Rev. Earth Planet. Sci.* 34, 217–262.
- Van Stempvoort, D.R., Krouse, H.R., 1994. Controls of d18O in sulfate: review of experimental data and application to specific environments. In: Alpers, C.N., Blowes, D.W. (Eds.), *Environmental geochemistry of sulfide oxidation*. Am. Chem. Soc., Washington DC.
- Wallace, P., 2001. Volcanic SO₂ emissions and the abundance and distribution of exsolved gas in magma bodies. *J. Volcanol. Geotherm. Res.* 108, 85–106.
- Yang, W., Spencer, R.J., Krouse, H.R., 1997. Stable isotope compositions of waters and sulfate species therein, Death Valley, California, USA: implications for inflow and sulfate sources, and arid basin climate. *Earth Planet. Sci. Lett.* 147, 69–82.
- Zielinski, G.A., Mayewski, P.A., Meeker, L.D., Whitlow, S., Wickler, M.S., Taylor, K., 1996. Potential atmospheric impact of the Toba mega-eruption similar to 71,000 years ago. *Geophys. Res. Lett.* 23, 837–840.

1. Sulfate extraction from samples

In order to extract all soluble sulfates, samples weighting 40-80 g were placed in 1L polypropylene beaker containing diluted HCl (0.1M) with a ratio sample/acid usually of 1/5. The pH of the solution was monitored to be between 1 and 2 and for the carbonate-bearing samples, concentrated HCl was added in order to maintain the required pH. After 24 hours at room temperatures, the beakers were heated up at 50-60°C during 1-2 hours before filtration through filter paper. The filtered solution was collected in glass beakers which were left evaporating at 60-80°C on a hot plate. While the solution was evaporating, barium chloride (BaCl₂) was added to the solution in order to precipitate barite (BaSO₄). Usually, after few hours, a white barite powder precipitated; then an excess of BaCl₂ was added to the remaining solution to scavenge it completely of SO₄²⁻ ions for 1-2 hours. We noticed that the two-steps addition of BaCl₂ results in larger crystals (~7-10 μm) of BaSO₄ than a single stage addition of BaCl₂ to the pre-evaporated solution. The resultant barite powder was rinsed 3 times with deionized water and dried out in oven at 60-80°C. It is important to note that during all this process (~48 hrs), isotopic exchanges between water and sulfate are expected to be negligible (Van Stempvoort and Krouse, 1994), because SO₄²⁻ is not a labile anion at these conditions. The sulfate concentration was estimated from the weight of extracted barite from samples on known weight.

For 16 samples, barite was purified from nitrate contamination by dissolution-precipitation method using DTPA, since high Δ¹⁷O measured in barite samples from some studies was inferred as coming from absorbed nitrate contamination (e.g. Bao, 2006). Around 20 mg of barite powder was placed in 30 mL of diethylene triamine penta acetic acid (DTPA) solution (0.05M DTPA in 1 M NaOH). After 1-2 hours at room temperature the barite is totally dissolved. Then, we acidified the solution by adding few drops of concentrated HCl (12M) in order to reprecipitate all the barite within 1-2 hours. Few drops of BaCl₂ were also added to help the BaSO₄ reprecipitation. After decanting, the barite powder was rinsed 3 or 4 times with deionized water and dried out. It is noteworthy that DTPA is an N-bearing compound, therefore it is important to abundantly (at least 3-4 times) rinse the purified barite in order to remove all the DTPA from the solution before drying it out and thus preventing any N-contamination that could be due to the DTPA treatment itself. In such a case, the mass interference of NF⁺ on the mass 33 during the supposed “purified barite” analyses will falsely increased the Δ¹⁷O (see below).

In order to quantify the nitrate contamination we run our 6 sulfate samples dissolved in DTPA solution were also run on an ion chromatograph at the Department of Chemistry at the University of Oregon. The measured NO₃/(NO₃+SO₄) in ash samples are: 2.8wt.%, 2.4 wt.%, 0.7 wt.%, 0.7 wt.% and 0 wt.% and in one sediment: 0 wt.%.

Therefore, we performed two consecutive dissolution-precipitations of each barite powder to make sure that all nitrate occlusions was removed. However, as we demonstrate above the nitrate contamination is systematically lower than 3 wt.% in our samples and as we discuss below, the Δ¹⁷O measured in purified samples is, in the uncertainties, the same that what we measured in unpurified barite. Therefore we did not attempt to carry DTPA treatment for every sample.

2. Oxygen isotope analyses

Oxygen isotopes were analyzed in the Stable Isotope Laboratory at the University of Oregon. Molecular oxygen was extracted from 4-7 mg of barite powder by a 35W CO₂-laser using BrF₅ as reagent and purified from traces of the reagent cryogenically and through the boiling mercury diffusion pump. Extracted O₂ gas was then frozen on molecular sieve (zeolite

13Å) before being expanded into the bellows of a Finnigan MAT253 mass spectrometer and run in a dual inlet mode for 8 cycles.

Some samples were run in both single and double trap system in which O₂ gas was refrozen on the second 13Å sieve before being expanded into the mass spectrometer. In the later, the O₂ gas extracted from the sample was trapped in the first molecular sieve that was at liquid nitrogen temperature (-196°C). Then we removed the liquid nitrogen flask from the first trap to the second one. Progressively the O₂ gas was transferred from the first to the second trap leaving most impurities in the first molecular sieve. When all O₂ gas was trapped in the second molecular sieve, the liquid nitrogen flask was removed and the oxygen expanded into the mass spectrometer leaving most of the impurities left in the second molecular sieve. Between each samples, the two molecular sieves were heated up with a heat gun and left degassing for at least 10 minutes. This technique attempted to prevent any traces of nitrogen fluoride contamination leading to isobaric interference of NF⁺ ion on the mass 33 affecting ¹⁷O¹⁶O signal (e.g. Rumble III et al., 1997; Pack et al., 2007). The Background scanning of nitrogen masses was monitored on the mass 52 (NF₂⁺) and gave systematically, when detectable, less than 1-2mV. We determined that atmospheric nitrate contamination was not present in our high-vacuum laser line.

Sample duplicates, and replicates of barite international standard NBS127 (n = 7) and in-house standard (IBO4-13; n = 12) give a reproducibility (in 2σ) usually better than δ¹⁸O ± 0.6‰, δ¹⁷O ± 0.3‰ and Δ¹⁷O ± 0.05‰. The 35-45% O₂ yield during barite laser fluorination leads to low-δ¹⁸O values, therefore based on the certified δ¹⁸O value of NBS127 (δ¹⁸O = 8.6‰), we applied a correction factor of +8.01‰ for all analyzed samples. Notice that this correction does not affect Δ¹⁷O values, which is a mass-independent parameter. Day to Day variations were also monitored by the GMG garnet standard.

Sulfate extraction and oxygen isotope analysis was replicated for few samples in order to assess the external errors of the whole method. Repeated extractions from different aliquots of the same sample of ash or sediment give reproducibility (in 2σ) better than δ¹⁸O ± 1.2‰, δ¹⁷O ± 0.7‰ and Δ¹⁷O ± 0.1‰.

We performed measurements on 16 purified barite powders using the DTPA dissolution-precipitation method. The Fig.1 shows that all samples plot very close to the line 1:1, meaning that the differences in Δ¹⁷O between the purified and unpurified barite are minimal or insignificant (≤0.1‰ out of the analytical uncertainties in 2σ). It is noteworthy that Δ¹⁷O values of the purified barite samples are either identical or sometimes 0.1‰ lower than the unpurified one (Fig. 1). This negative deviation can be due to the removal of minor environmental nitrate contamination (<2-3wt.%).

In order to test the hypothesis of mass interference of NF⁺ on the mass 33 and to remove hypothetical NF₃ contaminant, we analyzed few (N=3) samples with a double molecular sieve (zeolite 13Å) trap system. The difference in Δ¹⁷O between the single and double sieve trap systems is negligible (<0.05‰; on the line 1:1 Fig. 1) for two of the analyzed samples. The sample having the highest difference (see the circled points in the Fig. 1) yielded Δ¹⁷O = +0.33‰, which is comparable to what we obtained for the DTPA purified barite (Δ¹⁷O = +0.40‰). If the contaminant nitrate was mass-independent, the ¹⁷O-excess due to this contamination would be homogenized in the O₂ gas during the fluorination and won't be removed by the double sieve trap system. However, in both methods, we are able to prevent the NF⁺ mass 33 interference, meaning that in this experiment the source of the Δ¹⁷O increase in the untreated sample come from the NF⁺ mass interference and not from the mass-independence of the contaminant nitrate. It is important to note that this nitrate contamination in ash samples can potentially slightly increase the Δ¹⁷O of less than 0.1‰ (out of the uncertainties) in a sample having Δ¹⁷O more than 10 times higher (1.25‰. Fig. 1). Therefore,

it won't drastically change our overall interpretations that are mainly based on the $\Delta^{17}\text{O}$ variations of 2.3‰ in the Lake Tecopa stratigraphic section.

Figure Caption

Figure 1: Comparison between unpurified and purified barite using the DTPA dissolution-reprecipitation method (Bao et al.2006) or purifying the O_2 gas on the fluorination line with a double molecular sieve trap system. The error bars are $\pm 0.1\text{‰}$ (overall analytical uncertainties in 2σ) for each point and the 1:1 line. This graph demonstrates that all data points plot on or very close to the 1:1 line, indicating the robustness of analyses of unpurified barite with a single molecular sieve trap.

